The Journal of Chemical Physics ARTICLE scitation.org/journal/jcp

Production of ultracold $^{85}Rb^{133}Cs$ molecules in the lowest ground state via the $B^1\Pi_1$ short-range state

Cite as: J. Chem. Phys. 151, 084303 (2019); doi: 10.1063/1.5108637
Submitted: 30 April 2019 • Accepted: 31 July 2019 •
Published Online: 26 August 2019

Yuting Liu,[1,2] Ting Gong,[1,2] Zhonghua Ji,[1,2,a)] Gaoren Wang,[3] Yanting Zhao,[1,2,b)] Liantuan Xiao,[1,2] and Suotang Jia[1,2]

AFFILIATIONS

[1]State Key Laboratory of Quantum Optics and Quantum Optics Devices, Institute of Laser Spectroscopy, Shanxi University, Taiyuan 030006, China
[2]Collaborative Innovation Center of Extreme Optics, Shanxi University, Taiyuan, Shanxi 030006, China
[3]College of Physics, Dalian University of Technology, Dalian, Liaoning 116023, China

[a)]Electronic mail: jzh@sxu.edu.cn
[b)]Electronic mail: zhaoyt@sxu.edu.cn

ABSTRACT

We investigate the production of cold $^{85}Rb^{133}Cs$ molecules in the lowest vibronic level of the ground electronic state via the $B^1\Pi_1$ short-range state. The photoassociation (PA) spectra of the $B^1\Pi_1$ state, including newly observed transition to 2 vibronic levels, are obtained by high sensitivity time-of-flight mass spectrometry. Based on these PA spectra, the harmonic and anharmonic constants of vibronic states are obtained, resulting in predicted vibronic energies with an uncertainty of 1–2 cm^{-1}. The $B^1\Pi_1$ ($v = 3$) state is found to have the maximum production rate for ground-state molecules with a value of $3(1) \times 10^4$ s^{-1}, which is 3 times larger than the value via the previously studied $2^3\Pi_{0^+}$ ($v = 10$, $J = 0$) state with two-photon cascade decay. The populations of J = 0, 1, and 2 rotational levels of $X^1\Sigma^+$ ($v = 0$) state molecules formed via the $B^1\Pi_1$ ($v = 3$, $J = 1$) state are measured to be around 20%, 40%, and 20%. To quantify the coupling strength between the $B^1\Pi_1$ ($v = 3$) state and $X^1\Sigma^+$ ($v = 0$) state, the transition dipole moment between them is measured to be $7.2(2) \times 10^{-3} ea_0$, which is also 3 times larger than the value between the $2^3\Pi_{0^+}$ ($v = 10$) state and $X^1\Sigma^+$ ($v = 0$) state, meaning the $B^1\Pi_1$ ($v = 3$) state has a stronger coupling with the $X^1\Sigma^+$ ($v = 0$) state. Our detailed measurements provide relevant parameters for investigation on direct stimulated Raman adiabatic passage transfer between the atomic scattering state and molecular bound state for $^{85}Rb^{133}Cs$ molecules.

I. INTRODUCTION

Cold and ultracold molecules have attracted widespread attention of both physicists and chemists in the past two decades.[1–4] Compared with homonuclear molecules, heteronuclear (or polar) molecules have one distinctive property, which is tunable, long-range, and anisotropic dipole-dipole interaction. Due to this property, cold polar molecules have special applications in ultracold chemistry,[5,6] quantum computation,[7] quantum simulation,[8] and precision measurement.[9]

Molecules in the lowest vibronic ground state, i.e., $X^1\Sigma^+$ ($v = 0$), are especially important because they have the most stable quantum state and large dipole moments. Ground-state polar molecules have been produced by stimulated Raman adiabatic passage (STIRAP)[10] of Feshbach molecules[11–16] formed by magnetoassociation[17] or high vibronic state molecules[18] formed by photoassociation (PA).[19] Certain diatomic molecules can also be formed by direct laser cooling.[20–22] Among these methods, short-range PA is an interesting alternative method because of its ability to continuously produce and accumulate ground-state molecules and the possibility of adiabatical transfer of atomic scattering states to molecular bound states with STIRAP.[23,24] Several groups have successfully prepared ground-state molecules, including LiCs,[25] NaCs,[26] KRb,[27] RbCs,[28] and LiRb.[29] Among these systems, the RbCs molecule is especially

interesting because of its unique advantages. Due to its sizable permanent electric dipole moment,[30] RbCs is amenable to molecular alignment in the laboratory frame for quantum simulation.[8] The study on molecular Bose-Einstein condensation using RbCs is feasible due to the nonreaction of the ground state[31] and the avoidable immiscibility which is different from its isotopic components,[32] comparing with a degenerate Fermi gas of reactive polar molecules which need optical lattice to suppress chemical reaction.[11] In addition, purification of RbCs molecules in the rovibronic ground state has been proposed by using inelastic collision with the cotrapped Cs atom.[33]

Since the early investigations on the short-range PA to $2^3\Pi_{0^\pm}$ states of RbCs molecules,[28,34,35] the lowest ground-state molecules have been formed and detected with rotational resolution by using depletion spectroscopy[36] or microwave spectroscopy.[37] Shimasaki *et al.* found that the decays from the $2^3\Pi_{0^\pm}$ state of RbCs are two-photon cascade processes.[36] In comparison, for other investigated polar molecules, the PA state is the $B^1\Pi_1$ state and the spontaneous decay from this state is a single-step process.[25–27,29] The two-step nature of the spontaneous decay process of RbCs possesses an obstacle to realize stimulated Raman process and even STIRAP for enhancing the production rate of cold molecules in the selected quantum state. Thus, it is important to search more intermediate excited states that have mixed singlet-triplet characters. Such states have considerable Frank-Condon (FC) factors for transition between scattering states of atoms and deeply bound state of molecules. Shimasaki *et al.* first studied the $2^1\Pi_1$, $2^3\Pi_1$, and $3^3\Sigma_1^+$ states of RbCs molecules. These three states have the same total angular momentum projection along the internuclear axis ($\Omega = 1$) and hence are expected to be coupled by strong spin-orbit interaction.[38] It is found that the $2^1\Pi_1$ state has a relatively strong production rate for most lines, indicating that the singlet component plays an important role in short-range PA. This is similar to the case for other polar molecules where $B^1\Pi_1$ has a dominant singlet character and is simultaneously resonantly coupled to neighboring electronic states.[25–27,29] In 2013, Birzniece *et al.* investigated the Fourier-transform spectroscopy of the $B^1\Pi_1$ state of RbCs molecules. The transition frequencies as a function of internuclear separation demonstrate a clear "kink" due to perturbation or resonant coupling from other states.[39] Motivated by this possibility of single spontaneous decay, Shimasaki *et al.* recently investigated deeply bound rovibronic levels of the strongly perturbed $b^3\Pi_1 - c^3\Sigma_1^+ - B^1\Pi_1$ states in the vicinity of the perturbation. They observed $v = 5, 6, 10$ vibronic states in the PA spectra of the 4(1) state, which adiabatically correlates with the $B^1\Pi_1$ state, along with other electronic states. With the expectation that population on certain vibronic levels of the singlet $B^1\Pi_1$ state decay to the ground state primarily via the direct (one-photon) process just like other polar molecules, one wants to comprehensively investigate this state spectroscopically.

In this paper, we present extensive PA spectra of the $B^1\Pi_1$ state, in which all vibronic states with considerable Franck-Condon (FC) factors are observed, including 2 new vibronic states. Molecule constants for potential energy curves (PECs) are obtained in fitting these PA spectra and allow prediction of vibronic states that have not been experimentally accessed. The maximum molecule production rate of $3(1) \times 10^4$ s^{-1} was obtained using the $v = 3$ vibronic state. In the depletion spectroscopy, we also measured population distribution of formed lowest vibronic states via the $B^1\Pi_1$ ($v = 3$, J = 1) level and the transition dipole moment (TDM) between the upper and lower levels.

II. EXPERIMENT

Principles of the formation and detection of ultracold RbCs molecules in the lowest vibronic level via the $B^1\Pi_1$ state is shown in Fig. 1. The potential energy curves (PECs) are adopted from Refs. 40 and 41. The experimental setup was described in our previous publication on PA spectroscopy of the $(5)0^+$ state of RbCs.[42] However, in the present work, a different intermediate excited state was chosen. Furthermore, an additional depletion laser was used. Here, we only describe the main experimental processes with important experimental parameters.

In a vacuum chamber with a pressure of 3×10^{-6} Pa, 1×10^7 ^{85}Rb atoms in the $5S_{1/2}$ ($F = 2$) state (density = 8×10^{10} cm^{-3}) and 2×10^7 ^{133}Cs atoms in the $6S_{1/2}$ ($F = 3$) state (density = 1.5×10^{11} cm^{-3}) were produced using a dual-species dark spontaneous force optical trap (dark-SPOT). The temperatures of mixed atoms were measured by time-of-flight imaging to be both around 100 μK. A pair of colliding ^{85}Rb and ^{133}Cs atoms were photoassociated into the $B^1\Pi_1$ state in a short range, which is adiabatically correlated with the 4(1) state and the Rb($5S_{1/2}$) + Cs($6P_{3/2}$) dissociation limit at a long range. The photoassociated laser was provided by a tunable Ti:sapphire laser system (Sols Tis, M Squared) with a typical linewidth of 100 kHz and an output power of up to ~500 mW at 970–995 nm. We focused the PA beam on the center of the overlapped dark-SPOTs with a Gaussian radius of 500 μm. The weakly bound molecule is not stable and decays to the $X^1\Sigma^+$ state. Ground-state molecules were detected by one-color resonance-enhanced two-photon ionization (RETPI).[43] The photoionization laser is a pulse dye laser (CBRG-18EG, Spectra physics, pulse duration ~7 ns)

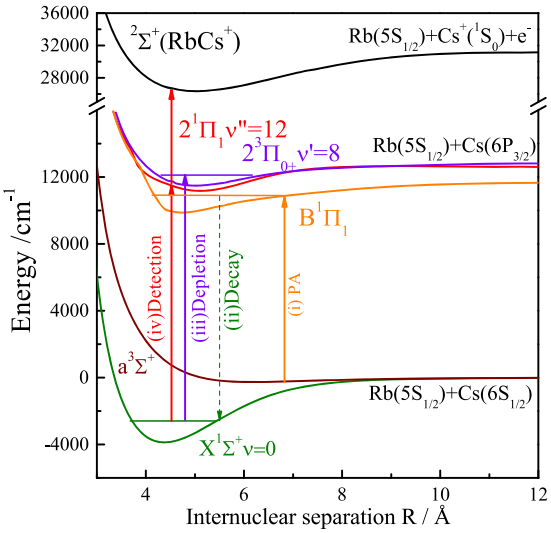

FIG. 1. Formation and detection mechanism of ultracold $X^1\Sigma^+$ ($v = 0$) state ^{85}Rb^{133}Cs molecules formed via the $B^1\Pi_1$ state.

pumped by the second harmonic of an Nd:YAG laser (INDIE-40-10-HG, Spectra physics), running at 10 Hz repetition rate. The wavelength of the pulsed dye laser was fixed at 651.8 nm to photoionize the $v = 0$ ground state molecules via the $2^1\Pi_1$ ($v = 12$) state, and the pulse energy was kept low (about 1 mJ) to avoid off-resonance excitation.[44] The photoionized ions were accelerated by an electric field (100 V/cm) and detected by a microchannel-plate, followed by a power amplifier. The ion signal was integrated and averaged by a Boxcar (SRS-250) every 10 shots. A depletion laser was introduced to measure the rotational distribution of RbCs molecules on the lowest vibronic level and the transition dipole moment between the $B^1\Pi_1$ and $X^1\Sigma^+$ states. The maximum power and typical irradiated time of the depletion laser were 7 mW and 2 ms, respectively.

III. RESULTS

In order to measure PA spectra of the $B^1\Pi_1$ state, PA laser frequency was scanned with a speed of 10 MHz/s around the estimated positions based on Refs. 45–47, while the pulsed photoionization (PI) laser frequency was fixed. Figure 2 shows our measured PA spectra of the $B^1\Pi_1$ state, in which $v = 3$ and 4 vibronic levels are observed for the first time and $v = 8$ and 9 levels are reassigned. For each observed level, the scanning range of the PA laser frequency is at least ±3 cm^{-1} in order not to miss levels. In Ref. 45, the $v = 8$ and 9 levels are assigned to the 2(1) state and the 3(1) state, respectively, implying that these two states overlap with the 4(1) state at these two levels. In Hund's case (a) and case (c) coupling schemes, the total angular momentum (excluding the nuclear spin) J is a combination of the rotational angular momentum R and projection of the total electron angular momentum $\Omega = \Lambda + \Sigma$, where Λ and Σ are the projection of the orbital (L) and spin (S) angular momenta, respectively. [Strictly speaking, Λ and Σ are not good quantum numbers in the case (c) coupling scheme]. Ω equals to 1 for 2(1), 3(1), and 4(1) states. Hyperfine structures complicate the PA spectra. No effort was taken to analyze or simulate the hyperfine structure. Instead, the frequency of the maximum-intensity transition of a hyperfine structure is taken as the rotational transition frequency. PA laser frequencies in the figures in the present paper are relative to that of the maximum-intensity transition to the $J = 1$ level for each vibronic state.

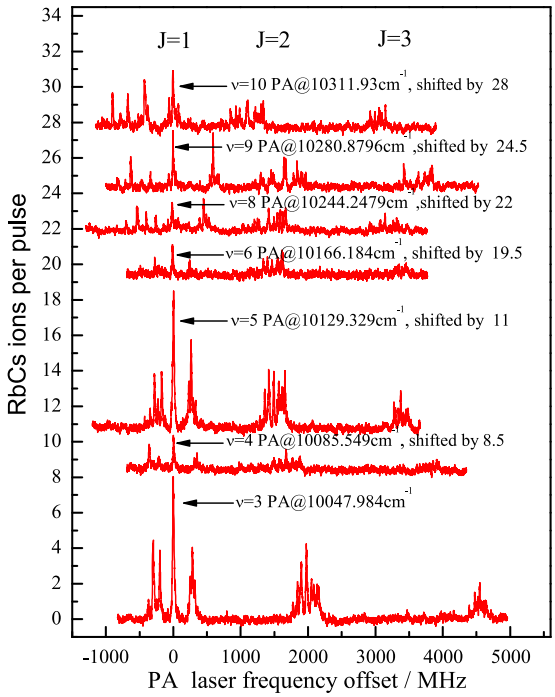

FIG. 2. PA spectra of the $B^1\Pi_1$ state. The PA laser frequency for the maximum intensity transition to the $J = 1$ level of each vibronic state is labeled and set to be the origin of the x axis. The shifted amount of the photoionized molecule number per pulse is also labeled for each spectrum.

Energies of rovibronic levels $E(v, J)$ of a diatomic molecule in the short-range region can be written as[48]

$$\frac{E}{hc} = T_e + \omega_e\left(v + \frac{1}{2}\right) - \omega_e\chi_e\left(v + \frac{1}{2}\right)^2 + B_e[J(J+1)] + D_e[J(J+1)]^2 - \alpha_e(v + 1/2)[J(J+1)], \quad (1)$$

where h is the Planck constant, c is the speed of light, T_e is the frequency spacing between the minimum point of the PEC and a reference energy level. Here, the well-known lower hyperfine states of ^{85}Rb and ^{133}Cs atoms are chosen to be the reference levels.[49,50] Its frequency spacing relative to the minimum point of the X state potential is 3836.141 cm^{-1} based on the measured value of dissociation energy.[51] The second and third terms on the right-side of Eq. (1) are harmonic and anharmonic terms of vibronic levels, respectively. The fourth and fifth terms are the rigid rotor and centrifugal stretching terms of rotational states, respectively. The last term represents the vibration-rotation effect. At the beginning, we used the normal RKR method[52] to fit the Dunham coefficients[53] and derived molecular constants in Eq. (1) but found that the one-standard-deviation error bars of fit values for the last three molecular constants (B_e, D_e, α_e) are larger than their absolute values. This is attributed to the fact that hyperfine structures are not simulated and hyperfine-structure-free transition frequencies are undetermined. Thus, we kept only the first three terms in Eq. (1) in deriving molecular PEC parameters. The fitted values are shown in Fig. 3(a) where the values of $J = 1$ rotational levels for all observed vibronic states are plotted and the molecular potential coefficients are derived as $\omega_e = 46.17(1)$ cm^{-1}, $\omega_e\chi_e = 0.569(1)$ cm^{-1}, and $T_e = 9891.70(1)$ cm^{-1}. Residuals of fitting the observed vibronic energies are shown in Fig. 3(a). Energies of unobserved vibronic states can be predicted with an uncertainty of 1–2 cm^{-1}.

The intensities of detected ion signals in Fig. 2 are quantified by our previous measurement of single ion.[54] Except for the spectrum of transitions to the $v = 3$ level, PA spectra are offset for clarity. The detected ion signal is proportional to the product of two FC factors. The first FC factor is between the atomic scattering state and the molecular excited state, called the free-bound factor in short, while the other is between the molecular excited state and its ground state, called the bound-bound factor in short. In Table 6.1 of Ref. 47, the author calculated these two factors for the $B^1\Pi_1$ excited bound states ranging from $v = 0$–15, shown in Fig. 3(b). To compare these

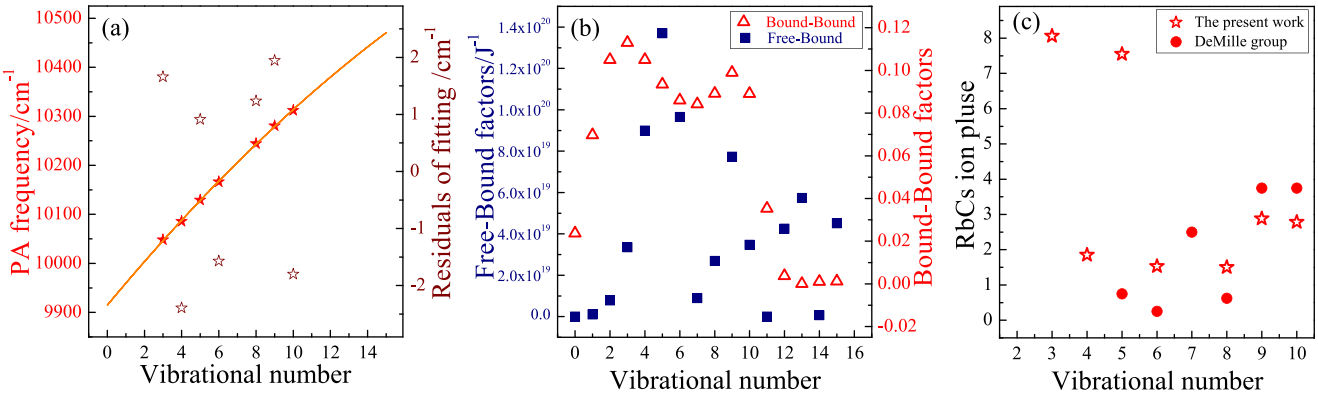

FIG. 3. (a) Energies of $J = 1$ rotational levels of observed vibronic states (left vertical axial) and residual of fitting to Eq. (1) with first three terms (right vertical axial). (b) The calculated FC factors for the free-bound (solid square) and bound-bound (hollow square) transitions to vibronic levels of the $B^1\Pi_1$ state in Ref. 47. (c) Numbers of RbCs ions per pulse for vibronic states observed in the present work (hollow pentacles) and by the DeMille group (solid circles).

theoretical calculations with the experimental measurement, we plot the quantified molecular intensity of PA transitions to $J = 1$ levels observed in the present work and in Ref. 45 in Fig. 3(c). It is worth noting that transition intensities are normalized by the formed molecules via the $2^3\Pi_{0^+}$ ($v = 10$, $J = 0$) PA level in both Ref. 45 and the present work. From Fig. 3(c), we see that in our measurement transitions to the $v = 3$ and 5 states have larger intensities than others (8.06 and 7.55 per pulse, respectively). The large ion-production rate via the v = 3 level is mainly due to the strong bound-bound transition, while the large ion-production rate via the v = 5 level is mainly attributed to the strong free-bound transition. By comparing the product of these two FC factors and our observations, we found that we have observed all the vibronic states with minimum combined FC factors of 1×10^{18}/J.

The quantification of the molecular ion signal also allows us to estimate the production rate of ground-state molecules. According to the relationship between the molecule production rate R and the number of photoions per pulse N_{ion},[55]

$$R = N_{ion}/\tau_c\eta, \tag{2}$$

where τ_c is the characteristic time of formed molecules with a value of 10 ms and η is the gross efficiency with a value of 3(1)% in our experiment.[54] The largest production rate of RbCs molecules in the lowest vibronic state is determined to be $3(1) \times 10^4$ s^{-1} when the PA laser frequency is locked to the $B^1\Pi_1$ ($v = 3$, $J = 1$) state. This value is 3 times larger than the value via the $2^3\Pi_{0^+}$ ($v = 10$, $J = 0$) level, in which two-photon cascade decay occurs.[54]

Because the linewidth of the PI laser is larger than the energy spacing of rotational levels, it is impossible to distinguish rotational distribution by RETPI. Thus, the depletion spectroscopy technique[56] was used to measure the rotational distribution when PA laser frequency is locked to the $B^1\Pi_1$ ($v = 3$, $J = 1$) state and PI laser is fixed at the transition between the $X^1\Sigma^+$ ($v = 0$) and $2^1\Pi_1$ ($v'' = 12$) states. The depletion laser frequency is scanned around the rotational transitions between the $X^1\Sigma^+$ ($v = 0$) and $2^3\Pi_{0^+}$ ($v' = 8$) states. Once the depletion laser is on-resonance with the transition, population on the lower level is depleted. To enhance the population depletion, the power of the depletion laser is set to the maximum value of 7 mW during the measurement. Figure 4 shows the depletion spectra and the rotational transitions for $J = 0$, 1, 2 levels of the $X^1\Sigma^+$ ($v = 0$) state. The depletion ratio, representing the population distribution, accounts for around 20%, 40%, and 20% for the three rotational levels, respectively. The uncertainty for the depletion ratios is less than 10%. It is worth noting no population on the $X^1\Sigma^+$ ($v = 0$, $J = 3$)

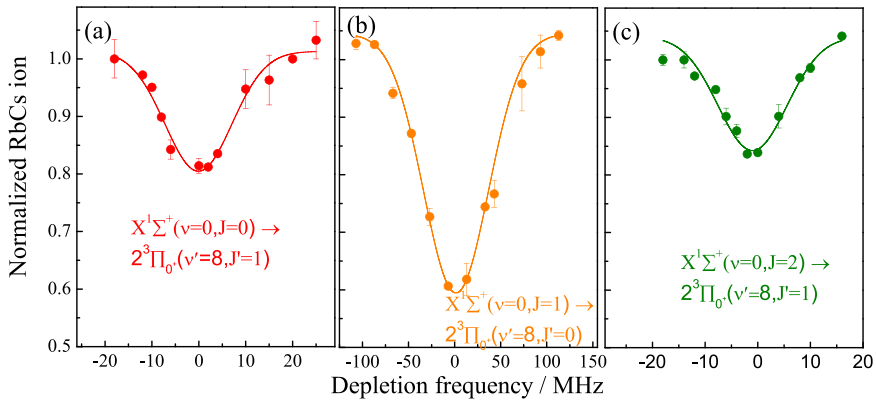

FIG. 4. Rotational distribution measurement of $^{85}Rb^{133}Cs$ molecules in the $X^1\Sigma^+$ ($v = 0$) state for $J = 0$ (a), $J = 1$ (b), and $J = 2$ (c) rotational levels when the PA laser is locked to the $B^1\Pi_1$ ($v = 3$, $J = 1$) level and the PI laser is fixed at the transition between the $X^1\Sigma^+$ ($v = 0$) and $2^1\Pi_1$ ($v'' = 12$) state.

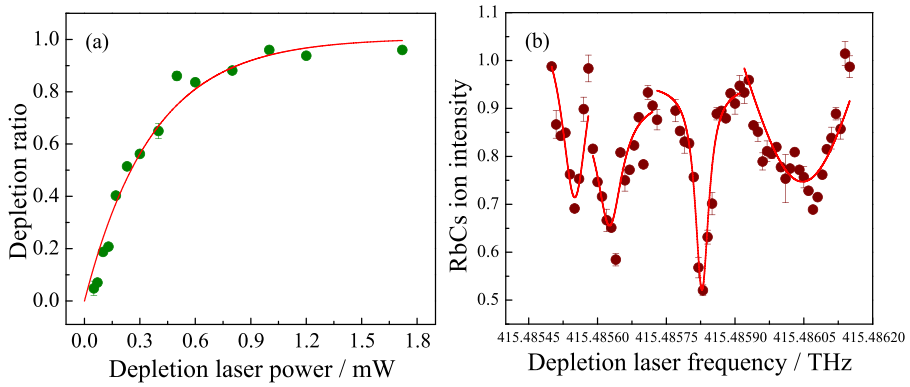

FIG. 5. (a) Dependence of the depletion ratio on depletion laser power for rotational transition between the $1^1\Pi_1$ ($v = 3$, $J = 1$) and the $X^1\Sigma^+$ ($v = 0$, $J = 1$) levels. The red curve is a fit to Eq. (3). (b) The depletion spectrum of transition between the $B^1\Pi_1$ ($v = 3$, $J = 1$) and the $X^1\Sigma^+$ ($v = 0$, $J = 1$) levels with the depletion laser power set at 0.01 mW.

level was detected. Besides the depletion laser power, there are other parameters that may affect the measurement of the depletion ratio, including off-resonance excitation induced by the PI laser and fluctuation of the background ion signal in the RETPI progress. Thus, it is unsurprising that the total depletion ratio is not unity. Considering the production rate of ground-state molecules, the corresponding rotational production rates for $J = 0$, 1, 2 are $0.6(3) \times 10^3$ s^{-1}, $1.2(4) \times 10^4$ s^{-1}, $0.6(2) \times 10^3$ s^{-1}, respectively. The central frequencies are 466.860 22, 466.858 59, and 466.857 50 THz, respectively, determined in fitting the spectral lineshapes to a Gaussian function [see Figs. 4(a)–4(c)]. They are also chosen to be the origin of x axial for each graph, i.e., the zero-point for relative frequencies. The absolute uncertainty for the center frequencies is 60 MHz limited by precision of the wavelength meter (High Finesse, WS-7R).

To quantify the coupling strength between the $B^1\Pi_1$ ($v = 3$) and $X^1\Sigma^+$ ($v = 0$) states, the depletion spectroscopy was also utilized to measure the transition dipole moment (TDM) between them. The related molecular states in the TDM measurement are different from the rotational distribution measurement. The depletion laser was used to couple these two states, while the PA laser was chosen to be locked to the transition to the $2^3\Pi_{0^-}$ ($v = 11$, $J = 0$) level in which the formed RbCs molecules populate only in the $X^1\Sigma^+$ ($v = 0$, $J = 1$) level.[36] Figure 5(a) shows the dependence of the depletion ratio on the power of the depletion laser when its frequency is on resonance with the transition between the $B^1\Pi_1$ ($v = 3$, $J = 1$) and $X^1\Sigma^+$ ($v = 0$, $J = 1$) states. The irradiated time t_i is 2 ms. When on resonance, the depletion ratio R_d can be written as[57]

$$R_d = 1 - e^{\frac{-2t_i\mu^2 P}{\pi\hbar^2\omega^2\gamma cn\varepsilon_0}} = 1 - e^{\frac{-P}{P_c}}, \tag{3}$$

where $\hbar$ is the reduced Planck constant, n is the refractive index (approximately equal to 1 for electromagnetic field propagation in vacuum), ε_0 is the permittivity of free space, ω is the waist of depletion laser and measured to be 1 mm, μ is the transition dipole moment, and P is the power of the depletion laser. $P_c = \pi\hbar^2\omega^2\gamma cn\varepsilon_0/2t_i\mu^2$ is the characteristic power and is determined to be 0.39(4) mW in fitting data with Eq. (3). γ is the lifetime broadening and is approximated by the linewidth of the depletion spectrum when the depletion laser power is much smaller than the characteristic power and power broadening is negligible. Figure 5(b) shows the depletion spectrum of transitions between the $X^1\Sigma^+$ ($v = 0$, $J = 1$) and the $B^1\Pi_1$ ($v = 3$, $J = 1$) levels where the power and interaction time are 0.01 mW and 0.2 ms, respectively. The observed 4 dips match the four hyperfine transitions in the PA spectrum of $B^1\Pi_1$ ($v = 3$, $J = 1$) rotational levels shown in Fig. 2. Fitting the lineshapes in the depletion spectrum with a multipeak Lorentzian function, γ is determined to be 40(1) MHz for the maximum-intensity transition. Substituting all experimentally determined values for parameters and physical constants into the expression of the characteristic power, the TDM between $1^1\Pi_1$ ($v = 3$, $J = 1$) and $X^1\Sigma^+$ ($v = 0$, $J = 1$) is derived to be $7.2(2) \times 10^{-3} ea_0$. This value is 3 times larger than the value between the $2^3\Pi_{0^+}$ ($v = 10$, $J = 2$) and $X^1\Sigma^+$ ($v = 0$, $J = 1$) levels.

IV. DISCUSSION ON POTENTIAL ATOM-MOLECULE STIRAP

In this section, we provide an estimation of the atom-molecule STIRAP efficiency with the $B^1\Pi_1$ ($v = 3$) state as the intermediate state, shown in Fig. 6(a). Besides the PA laser (i.e., the pump laser in STIRAP), an additional Stokes laser is required in STIRAP. To achieve the maximum transfer efficiency, the adiabatic condition below needs to be satisfied[58]

$$\frac{\Omega_0^2}{\pi^2\gamma} \gg \frac{1}{\tau} \gg D. \tag{4}$$

In these two inequalities, Ω_0 is the reduced Rabi frequency, γ is the lifetime broadening due to the excited intermediate state, τ is the pulse duration of pump and dump lasers (assumed to be the same), and D is the linewidth associated with the frequency difference between the two lasers. According to this definition, $\Omega_0 = \sqrt{\Omega_p^2 + \Omega_s^2}$, where Ω_p and Ω_s are the available maximum Rabi frequencies of the pump and Stokes transitions, respectively. For Stokes transition, we have measured the corresponding TDM $\mu_s = 7.2(2) \times 10^{-3} ea_0$ before and Ω_s can be obtained by $\Omega_s = \sqrt{2\mu_s^2 P_s/cn\varepsilon_0\pi\omega_s^2\hbar^2}$. Substituting available power $P_s = 1$ W and waist $\omega_s = 50$ μm of the focused beam, Ω_s can reach 179(6) MHz. To obtain the TDM between the atomic state and the molecular excited state μ_p, we measured the intensity of formed molecular ions as a function of PA laser power, shown in Fig. 6(b). This interaction between light and a two-level system with spontaneous decay

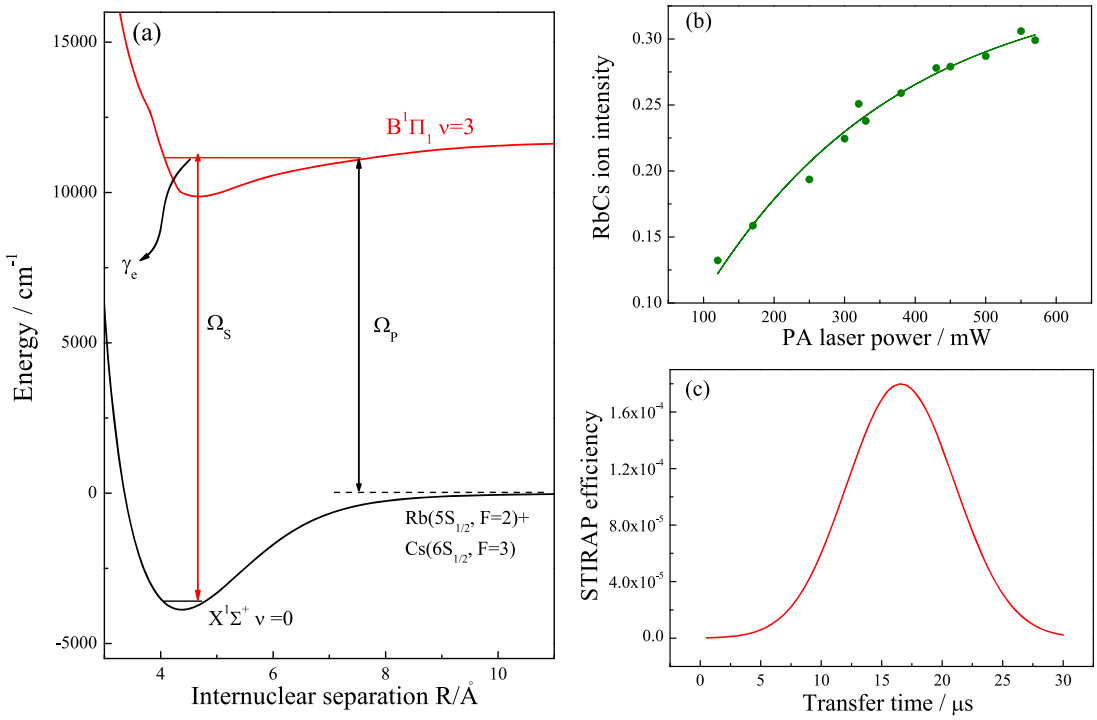

FIG. 6. (a) Scheme for atom-molecule STIRAP (see text for details). (b) The dependence of formed molecular ions on PA laser power in the absence of a dump laser with aim to derive the atom-molecule TDM. The curve is fitted to Eq. (3). (c) The calculated STIRAP efficiency as a function of transfer time when the pulse duration is 10 μs.

is similar to the depletion process; thus, Eq. (3) is also valid. The characteristic power is determined to be 277(19) mW. The beam waist of the PA laser is 50 μm, and the irradiated time is 90 ms; thus, μ_p is 4.0(1) $\times$ $10^{-6} ea_0$, which is 3 orders of magnitude lower than μ_s. Considering that the pump laser power P_p is 500 mW and the beam waist ω_p is 50 μm, $\Omega_p = \sqrt{2\mu_p^2 P_p / cn\varepsilon_0 \pi \omega_p^2 \hbar^2}$ is calculated to be 71(5) kHz. Thus, Ω_0 is dominated by Ω_s. Using the measured value of γ = 40(1) MHz, we can obtain that the pulse duration $\tau \gg 0.012$ μs according to the first inequality in Eq. (4). With experimental techniques currently available, linewidths of STIRAP lasers can be reduced to the kilohertz level by locking them to an ultra-low expansion cavity.[59] Thus, the second inequality in Eq. (4) requires $\tau \ll 1$ ms. Combining these two inequalities, the suitable duration τ is between 1 and 10 μs. We calculated the STIRAP efficiency when the duration is 1 and 10 μs. It is expected that longer durations help improving the efficiency. Figure 6(c) shows the calculated STIRAP efficiency as a function of transfer time when both duration times are 10 μs. The pulses of both pump and dump lasers are chosen to be Gaussian as usually the case in the experiment.[11–16] The transfer time refers to the time interval between the maxima of the Gaussian pulses. In the calculation, both single-photon resonance and two-photon resonance conditions are assumed. In Fig. 6(c), the optimal STIRAP efficiency appears at the transfer time of 16.5 μs which is larger than the pulse duration of the laser τ. This is due to the fact that the Rabi frequency Ω_s between the bound-bound transitions is three orders of magnitude larger than Ω_p between the free-bound transitions. Even though the transfer time is larger than the width, the Stokes laser pulse is strong enough to induce population transfer. It is shown in our calculation that the maximum STIRAP efficiency is around 0.02%. Starting with ~10^7 atoms, we expect to transfer ~2000 ground-state molecules. Comparing with the spontaneous decay of short-range PA, the production can be accomplished in tens of microseconds and the rovibrational level is selectable. Comparing with the case of Feshbach STIRAP,[11–16] this production rate is on the same order of magnitude but without the need of magnetoassociation which may be unsuitable for some molecular species. However, we expect to have more transferred molecules if the temperature of atomic samples can be decreased through common sub-Doppler cooling methods.

V. CONCLUSIONS

We report formation of $^{85}Rb^{133}Cs$ molecules in its lowest vibronic state via the short-range $B^1\Pi_1$ state. The PA spectra of the $B^1\Pi_1$ state, including 2 newly accessed vibronic states (v = 3 and 4), were obtained by high-sensitivity time-of-flight mass spectrometry. We determined the molecular constants in fitting these PA spectra: ω_e = 46.17(1) cm^{-1}, $\omega_e\chi_e$ = 0.569(1) cm^{-1}, and T_e = 9891.70(1) cm^{-1}. Based on these fitted parameters, energies of unobserved vibronic states have been derived with an uncertainty of 1–2 cm^{-1}. The maximum production rate for $^{85}Rb^{133}Cs$ molecules in the lowest vibronic state, 3(1) $\times$ 10^4 s^{-1}, has been found using the $B^1\Pi_1$ (v = 3) state as the intermediate state. This is 3 times larger

than the production rate via the $2^3\Pi_{0^+}$ ($v = 10$, $J = 0$) state with $1.2(4) \times 10^4$ s^{-1}. The populations of the $J = 0$, 1, and 2 rotational levels of $X^1\Sigma^+$ ($v = 0$) state molecules formed via the $B^1\Pi_1$ ($v = 3$, $J = 1$) state are measured to be around 20%, 40%, and 20%, respectively.

TDM between the $B^1\Pi_1$ ($v = 3$, $J = 1$) state and the $X^1\Sigma^+$ ($v = 0$, $J = 1$) state is measured to be $7.2(2) \times 10^{-3} ea_0$, which is 3 times larger than that between the $2^3\Pi_{0^+}$ ($v = 10$, $J = 2$) state and $X^1\Sigma^+$ ($v = 0$, $J = 1$) state. In Ref. 18, the spontaneous-decay-induced double resonance spectrum was observed in a Lambda system formed by the PA spontaneous decay molecular state, molecular excited state, and molecular ground state. The TDM between the latter two molecule states is as low as $9.8 \times 10^{-3} ea_0$, but two-photon dark resonance and coherent transfer between the PA spontaneous decay molecular state and molecular ground state are still observable. The TDM between the $X^1\Sigma^+$ ($v = 0$, J = 1) and $1^1\Pi_1$ ($v = 3$, J = 1) states has a similar amplitude, so it would be interesting to investigate the atom-molecule STIRAP in the future based on our estimation of the transfer efficiency.

ACKNOWLEDGMENTS

We acknowledge Dr. J. Liu from the University of Louisville for the help during the revision process. This work was supported by the National Key R&D Program of China (Grant No. 2017YFA0304203), the Natural Science Foundation of China (Grant Nos. 61675120, 11434007, and 61875110), NSFC Project for Excellent Research Team (Grant No. 61121064), Shanxi "1331 Project" Key Subjects Construction, PCSIRT (No. IRT_17R70), 111 project (Grant No. D18001), and the Open program of State Key Laboratory of Quantum Optics and Quantum Optics Devices (Grant No. KF201814).

REFERENCES

[1] J. Ulmanis, J. Deiglmayr, M. Repp, R. Wester, and M. Weidemüller, Chem. Rev. **112**, 4890 (2012).
[2] G. Quéméner and P. S. Julienne, Chem. Rev. **112**, 4949 (2012).
[3] J. L. Bohn, A. M. Rey, and J. Ye, Science **357**, 1002 (2017).
[4] S. Moses, J. Covey, M. Miecnikowski, D. Jin, and J. Ye, Nat. Phys. **13**, 13 (2017).
[5] J. Rui, H. Yang, L. Liu, D. Zhang, Y. Liu, J. Nan, Y. Chen, B. Zhao, and J. Pan, Nat. Phys. **13**, 699 (2017).
[6] X. Ye, M. Guo, M. L. G. Martínez, G. Quéméner, and D. Wang, Sci. Adv. **4**, eaaq0083 (2018).
[7] K.-K. Ni, T. Rosenband, and D. D. Grimes, Chem. Sci. **9**, 6830 (2018).
[8] J. A. Blackmore, L. Caldwell, P. D. Gregory, E. M. Bridge, R. Sawant, J. Aldegunde, J. Mur-Petit, D. Jaksch, J. M. Hutson, B. E. Sauer, M. R. Tarbutt, and S. L. Cornish, Quantum Sci. Technol. **4**, 014010 (2018).
[9] V. Andreev, D. G. Ang, D. DeMille, J. M. Doyle, G. Gabrielse, J. Haefner, N. R. Hutzler, Z. Lasner, C. Meisenhelder, B. R. O'Leary, C. D. Panda, A. D. West, E. P. West, and X. Wu, Nature **562**, 355 (2018).
[10] N. V. Vitanov, A. A. Rangelov, B. W. Shore, and K. Bergmann, Rev. Mod. Phys. **89**, 015006 (2017).
[11] L. De Marco, G. Valtolina, K. Matsuda, W. G. Tobias, J. P. Covey, and J. Ye, Science **363**, 853 (2019).
[12] T. Takekoshi, L. Reichsöllner, A. Schindewolf, J. M. Hutson, C. R. Le Sueur, O. Dulieu, F. Ferlaino, R. Grimm, and H.-C. Nägerl, Phys. Rev. Lett. **113**, 205301 (2014).
[13] P. K. Molony, P. D. Gregory, Z. Ji, B. Lu, M. P. Köppinger, C. R. Le Sueur, C. L. Blackley, J. M. Hutson, and S. L. Cornish, Phys. Rev. Lett. **113**, 255301 (2014).
[14] J. W. Park, S. A. Will, and M. W. Zwierlein, Phys. Rev. Lett. **114**, 205302 (2015).
[15] M. Guo, B. Zhu, B. Lu, X. Ye, F. Wang, R. Vexiau, N. Bouloufa-Maafa, G. Quéméner, O. Dulieu, and D. Wang, Phys. Rev. Lett. **116**, 205303 (2016).
[16] T. M. Rvachov, H. Son, A. T. Sommer, S. Ebadi, J. J. Park, M. W. Zwierlein, W. Ketterle, and A. O. Jamison, Phys. Rev. Lett. **119**, 143001 (2017).
[17] C. Chin, R. Grimm, P. Julienne, and E. Tiesinga, Rev. Mod. Phys. **82**, 1225 (2010).
[18] K. Aikawa, D. Akamatsu, M. Hayashi, K. Oasa, J. Kobayashi, P. Naidon, T. Kishimoto, M. Ueda, and S. Inouye, Phys. Rev. Lett. **105**, 203001 (2010).
[19] K. M. Jones, E. Tiesinga, P. D. Lett, and P. S. Julienne, Rev. Mod. Phys. **78**, 483 (2006).
[20] D. J. McCarron, M. H. Steinecker, Y. Zhu, and D. DeMille, Phys. Rev. Lett. **121**, 013202 (2018).
[21] K. N. Jarvis, J. A. Devlin, T. E. Wall, B. E. Sauer, and M. R. Tarbutt, Phys. Rev. Lett. **120**, 083201 (2018).
[22] L. Anderegg, B. L. Augenbraun, E. Chae, B. Hemmerling, N. R. Hutzler, A. Ravi, A. Collopy, J. Ye, W. Ketterle, and J. M. Doyle, Phys. Rev. Lett. **119**, 103201 (2017).
[23] S. Stellmer, B. Pasquiou, R. Grimm, and F. Schreck, Phys. Rev. Lett. **109**, 115302 (2012).
[24] G. Reinaudi, C. B. Osborn, M. McDonald, S. Kotochigova, and T. Zelevinsky, Phys. Rev. Lett. **109**, 115303 (2012).
[25] J. Deiglmayr, A. Grochola, M. Repp, K. Mörtlbauer, C. Glück, J. Lange, O. Dulieu, R. Wester, and M. Weidemüller, Phys. Rev. Lett. **101**, 133004 (2008).
[26] P. Zabawa, A. Wakim, M. Haruza, and N. P. Bigelow, Phys. Rev. A **84**, 061401 (2011).
[27] J. Banerjee, D. Rahmlow, R. Carollo, M. Bellos, E. E. Eyler, P. L. Gould, and W. C. Stwalley, Phys. Rev. A **86**, 053428 (2012).
[28] C. D. Bruzewicz, M. Gustavsson, T. Shimasaki, and D. DeMille, New J. Phys. **16**, 023018 (2014).
[29] I. C. Stevenson, D. B. Blasing, Y. P. Chen, and D. S. Elliott, Phys. Rev. A **94**, 062510 (2016).
[30] M. Aymar and O. Dulieu, J. Chem. Phys. **122**, 204302 (2005).
[31] P. S. Żuchowski and J. M. Hutson, Phys. Rev. A **81**, 060703 (2010).
[32] D. J. McCarron, H. W. Cho, D. L. Jenkin, M. P. Köppinger, and S. L. Cornish, Phys. Rev. A **84**, 011603 (2011).
[33] E. R. Hudson, N. B. Gilfoy, S. Kotochigova, J. M. Sage, and D. DeMille, Phys. Rev. Lett. **100**, 203201 (2008).
[34] C. Gabbanini and O. Dulieu, Phys. Chem. Chem. Phys. **13**, 18905 (2011).
[35] Z. Ji, H. Zhang, J. Wu, J. Yuan, Y. Yang, Y. Zhao, J. Ma, L. Wang, L. Xiao, and S. Jia, Phys. Rev. A **85**, 013401 (2012).
[36] T. Shimasaki, M. Bellos, C. D. Bruzewicz, Z. Lasner, and D. DeMille, Phys. Rev. A **91**, 021401 (2015).
[37] Z. Li, Z. Ji, T. Gong, J. Cao, Y. Zhao, L. Xiao, and S. Jia, Opt. Express **26**, 2341 (2018).
[38] T. Shimasaki, J. T. Kim, and D. DeMille, ChemPhysChem **17**, 3677 (2016).
[39] I. Birzniece, O. Docenko, O. Nikolayeva, M. Tamanis, and R. Ferber, J. Chem. Phys. **138**, 154304 (2013).
[40] H. Fahs, A. R. Allouche, M. Korek, and M. Aubert-Frécon, J. Phys. B: At., Mol. Opt. Phys. **35**, 1501 (2002).
[41] A. R. Allouche, M. Korek, K. Fakherddin, A. Chaalan, M. Dagher, F. Taher, and M. Aubert-Frécon, J. Phys. B: At., Mol. Opt. Phys. **33**, 2307 (2000).
[42] J. Yuan, Y. Zhao, Z. Ji, Z. Li, J. T. Kim, L. Xiao, and S. Jia, J. Chem. Phys. **143**, 224312 (2015).
[43] Z. Li, Z. Ji, X. Zhang, J. Yuan, Y. Zhao, L. Xiao, and S. Jia, J. Phys. Soc. Jpn. **85**, 084301 (2016).
[44] Y. Zhao, J. Yuan, Z. Li, Z. Ji, L. Xiao, and S. Jia, Chin. Phys. Lett. **32**, 113301 (2015).
[45] T. Shimasaki, J. T. Kim, Y. Zhu, and D. DeMille, Phys. Rev. A **98**, 043423 (2018).
[46] T. Bergeman, A. J. Kerman, J. Sage, S. Sainis, and D. DeMille, Eur. Phys. J. D **31**, 179 (2004).
[47] T. Shimasaki, "Continuous production of $^{85}Rb^{133}Cs$ molecules in the rovibronic ground state via short-range photoassociation," Ph.D. thesis, Yale University, 2017.

[48]P. F. Bernath, *Spectra of Atoms and Molecules* (Oxford University Press , 1995).
[49]D. A. Steck, Rubidium 85 D Line Data, 2.1.6 ed., 2013, http://steck.us/alkalidata.
[50]D. A. Steck, Cesium D Line Data, 2.1.4 ed., 2010, http://steck.us/alkalidata.
[51]O. Docenko, M. Tamanis, R. Ferber, H. Knöckel, and E. Tiemann, Phys. Rev. A **83**, 052519 (2011).
[52]J. Banerjee, D. Rahmlow, R. Carollo, M. Bellos, E. E. Eyler, P. L. Gould, and W. C. Stwalley, J. Chem. Phys. **139**, 174316 (2013).
[53]J. L. Dunham, Phys. Rev. **41**, 721 (1932).
[54]Z. Ji, Z. Li, T. Gong, Y. Zhao, L. Xiao, and S. Jia, Chin. Phys. Lett. **34**, 103301 (2017).
[55]A. Fioretti, C. Amiot, C. Dion, O. Dulieu, M. Mazzoni, G. Smirne, and C. Gabbanini, Eur. Phys. J. D **15**, 189 (2001).
[56]D. Wang, J. T. Kim, C. Ashbaugh, E. E. Eyler, P. L. Gould, and W. C. Stwalley, Phys. Rev. A **75**, 032511 (2007).
[57]M. Debatin, T. Takekoshi, R. Rameshan, L. Reichsöllner, F. Ferlaino, R. Grimm, R. Vexiau, N. Bouloufa, O. Dulieu, and H. C. Nägerl, Phys. Chem. Chem. Phys. **13**, 18926 (2011).
[58]K. Aikawa, D. Akamatsu, J. Kobayashi, M. Ueda, T. Kishimoto, and S. Inouye, New J. Phys. **11**, 055035 (2009).
[59]P. D. Gregory, P. K. Molony, M. P. Köppinger, A. Kumar, Z. Ji, B. Lu, A. L. Marchant, and S. L. Cornish, New J. Phys. **17**, 055006 (2015).